# SHAPE FROM SHADING FOR HYBRID SURFACES

*Abdelrehim Ahmed and Aly Farag*

Computer Vision and Image Processing Laboratory (CVIP)
University of Louisville, Louisville, KY, 40292

## ABSTRACT

This paper presents a new method for recovering the shape of hybrid surfaces that have both diffuse reflection and specular reflection using shape from shading (SFS). The image irradiance equation has been derived as an explicit partial differential equation (PDE) under the assumptions of orthographic camera projection and distant point light source. The reflectance model of Ward has been used to express the hybrid reflection as a linear combination from the diffuse and specular components. The resulting PDE is solved using the Lax-Friedrichs sweeping method. The proposed algorithm is evaluated by using both synthetic data and real images and the experimental results show the efficiency of the approach.

***Index Terms***— Shape from Shading, Ward Model, Lax-Friedrichs sweeping.

## 1. INTRODUCTION

The shape from shading (SFS) problem is to analyze the brightness variation in a single image of a scene to recover the 3D-shape of that scene. SFS was formally introduced by Horn [1] who formulated the SFS problem by a nonlinear first order partial differential equation (PDE) called the *image irradiance equation*. This equation models the relation between the shape of an object and its image brightness under known illumination conditions. During the last three decades, a large number of different SFS approaches have emerged [2, 3, 4, 5, 6] (for survey see [7, 8])

In general, the brightness of a surface patch depends on its orientation relative to both the light source and the viewer. Under the simplifying assumption that the viewer and the light source are far from the object, the *image irradiance equation* can be written as follows:

$$E(\boldsymbol{x}) = \mathcal{R}(\hat{\boldsymbol{n}}(\boldsymbol{x})) \tag{1}$$

where $E(\boldsymbol{x})$ is the image irradiance at the point $\boldsymbol{x}$ and $\mathcal{R}(.)$ is the radiance of a surface patch with unit normal $\hat{\boldsymbol{n}}(\boldsymbol{x})$.

For simplification purposes, most of the existing SFS approaches, e.g., [4, 5, 9] assume that the object has a perfectly diffuse (Lambertian) surface. Under real world circumstances the surface materials are not perfectly diffuse nor perfectly specular. Most of real surfaces have a hybrid reflectance which can be approximated by a linear combination of specular reflectance and diffuse reflectance.

Modeling only the diffuse reflectance in the SFS image irradiance equation may lead to erroneous results when secularities are present since the specular highlights may be misinterpreted as high curvature surface features.

In the literature, only a small number of SFS algorithms have been proposed for surfaces with both specular and diffuse reflectance. One of these algorithms was presented by Lee and Kuo [10] where a generalized reflectance map was used. They discretized the image irradiance equation with a triangular element surface model which involved only the depth variables. The shape was computed by linearizing the resulting nonlinear equations and minimizing a quadratic energy functional. In addition to being computationally expensive, the given results for this method were not promising. According to their modeling, Lee and Kuo noticed that "the non-Lambertian surface can hardly be recovered correctly with two photometric stereo images" [10].

For shiny curved objects, Ragheb and Hancock [11] have developed a maximum a posteriori probability estimation method to estimate the mixing proportions for Lambertian and specular reflectance, and in the same time, to recover the surface orientation.

In this paper, we formulate the SFS problem for surfaces that have both diffuse and specular reflections using the hybrid reflectance model of Ward. The proposed algorithm can handel the extreme cases as well, i.e., Lambertian surfaces and very shiny surfaces.

## 2. WARD REFLECTANCE MODEL

The reflectance model proposed by Ward [12] is physically realizable variant of Phong model [13]. Ward's model accounts for both the diffuse and the specular components of the reflectance in a simple formula that is constrained to obey fundamental physical laws, such as conservation of energy and reciprocity. The model has been validated by collecting many measurements from real samples using a simple reflectometry device that was designed by Ward and the research team in Lawrence Berkeley Laboratory [12].

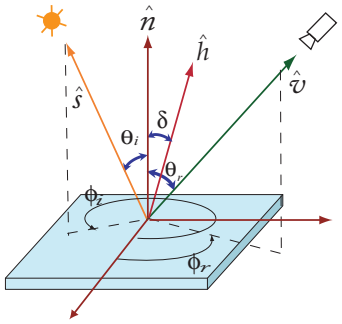


**Fig. 1**. Definitions of reflection parameters and angles. $\hat{\boldsymbol{h}} = (h_x, h_y, h_z) = \frac{\hat{\boldsymbol{s}}+\hat{\boldsymbol{v}}}{|\hat{\boldsymbol{s}}+\hat{\boldsymbol{v}}|}$.

The expression for Ward's reflectance model is given by:

$$L_r(\theta_i, \phi_i, \theta_r, \phi_r) = \frac{\rho_d \cos\theta_i}{\pi} + \rho_s \sqrt{\frac{\cos\theta_i}{\cos\theta_r}} \frac{\exp[-\tan^2\delta/\sigma^2]}{4\,\pi\,\sigma^2}; \quad (2)$$

where $\rho_d$ is the diffuse albedo and it determines the proportion of incoming light reflected diffusely. The higher the value of $\rho_d$, the brighter the surface. The specular albedo $\rho_s$ controls the proportion of incoming light that is reflected specularly. Small values of this parameter yield matte surfaces while higher values yield glossy and metallic surfaces. The parameter $\sigma$ is the standard deviation of the surface roughness at a microscopic scale. Changing this parameter leads to changes in the "spread" of the specular reflection. Small values of the roughness parameter lead to crisp specular reflections, while Large values lead to blurred reflections like unpolished metals. The angle $\delta$ is the angle between vector $\hat{n}$ and $\hat{h}$ as shown in Fig. 1.

## 3. THE IMAGE IRRADIANCE EQUATION FOR HYBRID SURFACES

In this section the SFS image irradiance equation for hybrid surfaces is derived using the following assumptions: (1) The object is far from the camera, therefore the camera projection can be approximated by an orthographic projection; (2) The scene is illuminated by a point light source located far away from the surface; (3) the surface reflectance is modeled by Eq. 2.

Assume that the compact domain $\Omega \subset \mathbb{R}^2$ is the image domain and $I : \Omega \to [0, 1]$ is the image intensity. The surface is represented by $\mathcal{S} = \{(\boldsymbol{x}, u(\boldsymbol{x})) \quad / \boldsymbol{x} \in \Omega\}$ where $u(\boldsymbol{x})$ is the surface height at point $\boldsymbol{x}$ above the $xy$ plane. The unit vectors $\hat{\boldsymbol{s}} = (s_x, s_y, s_z)$ and $\hat{\boldsymbol{v}} = (v_x, v_y, v_z)$ are used to specify the directions of the light and the camera respectively. The symbol $\boldsymbol{\tau_s}$ refers to the first two components of $\hat{\boldsymbol{s}}$. Similarly the symbol $\boldsymbol{\tau_v}$ refers to the first two components of $\hat{\boldsymbol{v}}$.

The unit normal vector at the point $\boldsymbol{x}$ on the surface is expressed as a function of the surface gradient as $\hat{\boldsymbol{n}}(\boldsymbol{x}) = (-\nabla u(\boldsymbol{x}), 1)/\sqrt{1+|\nabla u|^2}$.

From the geometry illustrated in Fig. 1, we derive the following expression for the irradiance equation:

$$I(x)\left[\frac{\sqrt{1+|\nabla u|^2}}{-\boldsymbol{\tau_s}\cdot\nabla u + s_z}\right] - \frac{\rho_d}{\pi} - \frac{\rho_s}{4\,\pi\sigma^2}\sqrt{\frac{1+|\nabla u|^2}{(-\boldsymbol{\tau_s}\cdot\nabla u + s_z)(-\boldsymbol{\tau_v}\cdot\nabla u + v_z)}} \times \exp\left[\frac{-1}{\sigma^2}\frac{(1+|\nabla u|^2) - (-\hat{\boldsymbol{\tau}}_{\boldsymbol{h}}\cdot\nabla u + h_z)^2}{(-\hat{\boldsymbol{\tau}}_{\boldsymbol{h}}\cdot\nabla u + h_z)^2}\right] = 0. \quad (3)$$

Note that the reflected radiance $L_r$ has been replaced by the measured image gray value $I$ by assuming a linear relationship between them and dropping the scaling factors.

### 3.1. Solving the proposed PDE

To solve the image irradiance equation ( 3) a powerful numerical tool is needed. One of the candidate tools is the Lax-Friedrichs Sweeping (LFS) method [14]. The main advantage of LFS method is its ability to deal with both convex and non-convex Hamiltonians with any degree of complexity. We used the LFS method in our previous work [15] to solve the SFS problem for a class of non-Lambertian diffuse surfaces and it shows a good peformance.

To solve a PDE with LFS method we should put it in the following form:

$$\begin{cases} H(\nabla u, \boldsymbol{x}) = R(\boldsymbol{x}) & \forall \boldsymbol{x} \in \Omega \\ u(\boldsymbol{x}) = \psi(\boldsymbol{x}) & \forall \boldsymbol{x} \in \partial\Omega, \end{cases} \quad (4)$$

Where $\psi$ is a Dirichlet boundary condition.

For Eq. 3 the expressions of $H$ and $R$ are given by:

$$H = I(x)\left[\frac{\sqrt{1+|\nabla u|^2}}{-\boldsymbol{\tau_s}\cdot\nabla u + s_z}\right] - \frac{\rho_s}{4\,\pi\sigma^2}\sqrt{\frac{1+|\nabla u|^2}{(-\boldsymbol{\tau_s}\cdot\nabla u + s_z)(-\boldsymbol{\tau_v}\cdot\nabla u + v_z)}} \times \exp\left[\frac{-1}{\sigma^2}\frac{(1+|\nabla u|^2) - (-\hat{\boldsymbol{\tau}}_{\boldsymbol{h}}\cdot\nabla u + h_z)^2}{(-\hat{\boldsymbol{\tau}}_{\boldsymbol{h}}\cdot\nabla u + h_z)^2}\right] = 0; \quad R = \frac{\rho_d}{\pi}. \quad (5)$$

In this work, we assume that the object is in front of a background that is used as a boundary condition with zero depth. The 2D version of the LFS method [14] is applied to recover the shape of the scene form the input image using the $H$ and $R$ expressions in Eq.5.

## 4. EXPERIMENTAL RESULTS AND DISCUSSION

In order to evaluate the performance of the proposed approach, we have conducted several experiments on both synthetic and

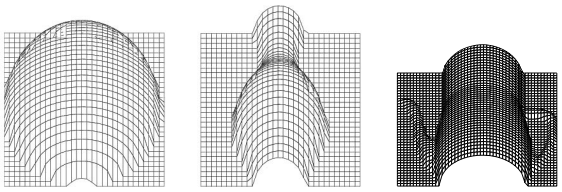

**Fig. 2**. Ground truth maps used to generate the synthetic images.

| image name | mean of the absolute error | standard deviation of the absolute error | mean of the gradient error |
|---|---|---|---|
| sphere (a) | 0.039 | 0.037 | 0.0026 |
| sphere (b) | 0.041 | 0.045 | 0.0031 |
| sphere (c) | 0.036 | 0.034 | 0.0026 |
| vase (a) | 0.022 | 0.035 | 0.0023 |
| vase (b) | 0.024 | 0.044 | 0.0030 |
| vase (c) | 0.037 | 0.058 | 0.0032 |
| pot (a) | 0.055 | 0.059 | 0.0030 |
| pot (b) | 0.070 | 0.063 | 0.0028 |
| pot (c) | 0.099 | 0.089 | 0.0031 |

**Table 1**. The error measures for the results in Fig. 3.

real images. The test set consists of three synthetic data sets and four real images. The synthetic images were generated using the depth map of a sphere, a vase and a synthetic pot as shown on Fig. 2. The maximum depth of all theses objects is normalized to one.

### 4.1. Synthetic images

For the quantitative analysis, we compare the recovered depth with the reference depth map (Fig. 2) and compute the mean and the standard deviation of the absolute error. We also provide the mean of the absolute error in the two gradient components. Figure 3 shows nine synthetic images and their corresponding shapes recovered by the proposed SFS. These synthetic images are generated using three different settings as detailed in the caption of Fig. 3. As can be clearly seen from the figure, and the error measures in Table 1, the shapes are recovered with very high precision for all cases. Even for images with large specular component (see column (c) of Fig. 3) the error is very small.

### 4.2. Real images

The applicability of the proposed SFS approach for real data is tested experimentally by using four real images for a metallic bar, a bottle, and a hair dryer. These images and their recovered shapes are shown on Fig. 4. For all cases, the parameter values of Ward model are selected manually.

As shown in Fig. 4, the shapes are recovered with good accuracy for all objects. In order to better judge the performance of the proposed algorithm, we used a Cyberware 3D scanner [16] to get a very accurate height map for the bottle. Figure 5 compares between the output of the 3D scanner and the estimated shape produced by the SFS algorithm using

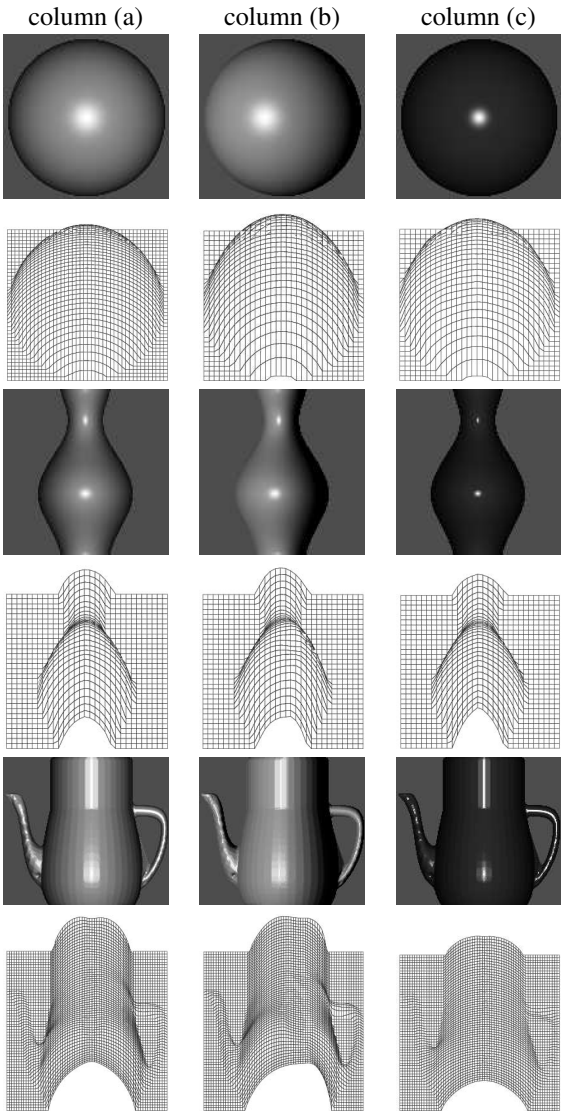


**Fig. 3**. Experiments on three sets of synthetic images: sphere, vase and pot. The synthetic images are displayed in the first, the third and the fifth row and their corresponding recovered shapes are displayed in the second, the fourth and the sixth row respectively. The images in column(a) are generated with $\boldsymbol{s = (0, 0, 1)}$, $\boldsymbol{\rho_d = 0.67}$, $\boldsymbol{\rho_s = 0.075}$ and $\boldsymbol{\sigma = 0.2}$. The images in column(b) are generated with $\boldsymbol{s = (-0.5, 0, 1)}$, $\boldsymbol{\rho_d = 0.67}$, $\boldsymbol{\rho_s = 0.075}$ and $\boldsymbol{\sigma = 0.2}$. The images in column(c) are generated with $\boldsymbol{s = (0, 0, 1)}$, $\boldsymbol{\rho_d = 1}$, $\boldsymbol{\rho_s = 0.2}$ and $\boldsymbol{\sigma = 0.1}$. For all cases $v = (0, 0, 1)$

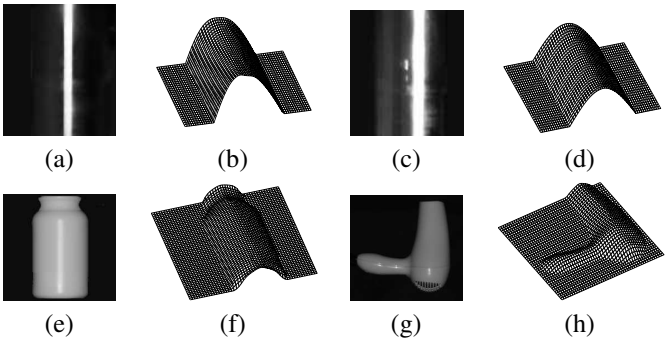

**Fig. 4**. Experiments on real images. (a) a metallic bar captured under $s = v = (0, 0, 1)$ (c) a metallic bar captured under $s = (0.5, 0, 1)$ and $v = (-0.2, 0, 1)$. (b,d) the recovered shapes of (a,c) respectively. (e,f) a bottle and its recovered shape. (g,h) a hair dryer and its recovered shape.

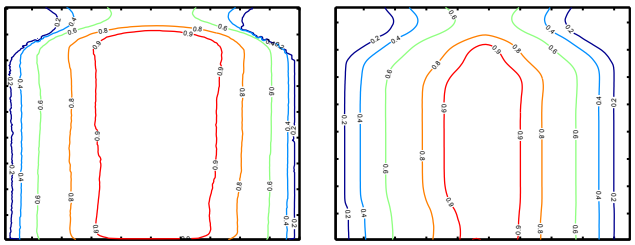

**Fig. 5**. Contour plot for the height map of the bottle: (a) using the height map produced by the Cyberware 3D scanner, (b)using the height map produced by the proposed SFS algorithm

contour plots. The height contours of the recovered shape in Fig. 5(b) is close to their corresponding contours in Fig. 5(a) which indicates the accuracy of the recovered shape.

## 5. CONCLUSION

In this paper we have formulated the SFS for hybrid surfaces that have combination of diffuse and specular reflections. Using the reflectance model of Ward and the assumptions of orthographic camera and distant light source, the image irradiance equation is derived. The resulting PDE is solved using a fast numerical algorithm based on Lax-Friedrichs sweeping method. The main advantage of this numerical algorithm is its capability of handling the complexity of the proposed PDE. The SFS algorithm is evaluated using both synthetic and real data sets and the experimental results show the potential of the approach.

## 6. ACKNOWLEDGEMENTS

This research has been supported by National Science Foundation (NSF) (Grant IIS-0513974)

## 7. REFERENCES

[1] B.K.P. Horn, *Shape from Shading: A Method for Obtaining the Shape of a Smooth Opaque Object from One View*, Ph.D. thesis, Massachusetts Inst. of Technology, Cambridge, Massachusetts, 1970.

[2] A.P. Pentland, "Local shading analysis," *IEEE Trans. on Pattern Analysis and Machine Intelligence*, vol. 6, no. 2, pp. 170–187, 1984.

[3] M.J. Brooks and B.K.P. Horn, "Shape and source from shading," in *Proceedings of the International Joint conference on Artificial Intelligence*, 1985, pp. 932–936.

[4] R.T. Frankot and R. Chellappa, "A method for enforcing integrability in shape from shading algorithms," *IEEE Trans. on Pattern Analysis and Machine Intelligence*, vol. 10, no. 4, pp. 439–451, 1988.

[5] E. Rouy and A. Tourin, "A viscosity solutions approach to shape from shading," *SIAM J. Numerical Analysis*, vol. 29, no. 3, pp. 867–884, 1992.

[6] E. Prados and O. Faugeras, "Shape from shading: a well-posed problem?," in *CVPR05*, San Diego, CA, USA, June 2005.

[7] R. Zhang, P.-S. Tsai, J.-E. Cryer, and M. Shah, "Shape from shading: A survey," *IEEE Trans. on Pattern Analysis and Machine Intelligence*, vol. 21, no. 8, pp. 690–706, 1999.

[8] J-D. Durou, M. Falcone, and M. Sagona, "A survey of numerical methods for shape from shading," 2004-2-r, Institut de Recherche en Informatique de Toulouse (IRIT), 2004.

[9] P.S. Tsai and M. Shah, "Shape from shading using linear approximation," *Image and Vision Computing J.*, vol. 12, no. 8, pp. 487–498, 1994.

[10] Kyoung Mu Lee and C.-C. Jay Kuo, "Shape from shading with a generalized reflectance map model," *Comput. Vis. Image Underst.*, vol. 67, no. 2, pp. 143–160, 1997.

[11] Hossein Ragheb and Edwin R. Hancock, "A probabilistic framework for specular shape-from-shading.," *Pattern Recognition*, vol. 36, no. 2, pp. 407–427, 2003.

[12] Gregory J. Ward, "Measuring and modeling anisotropic reflection," in *Proceedings of the 19th annual conference on Computer graphics and interactive techniques,SIGGRAPH'92*, 1992, pp. 265–272.

[13] Bui Tuong Phong, "Illumination for computer generated pictures," *Commun. ACM*, vol. 18, no. 6, pp. 311–317, 1975.

[14] C. Y. Kao, Stanley Osher, and J. Qian, "Lax-friedrichs sweeping scheme for static hamilton-jacobi equations," *Journal of Computational Physics*, vol. 196, no. 1, pp. 367 – 391, 2004.

[15] Abdelrehim H. Ahmed and Aly A. Farag, "A new formulation for shape from shading for non-lambertian surfaces," in *International Conference on Computer Vision and Pattern Recognition CVPR06*, NY, USA, 2006, pp. 1817–1824.

[16] Cyberware 3D scanners, "http://www.cyberware.com," .